Thèse de doctorat

NNT: 2020UPASA000

Propriétés catalytiques à l'échelle nanométrique sondées par diffraction des rayons X de surface et imagerie de diffraction cohérente.

Catalytic properties at the nanoscale probed by surface x-ray diffraction and coherent diffraction imaging

Thèse de doctorat de l'Université Paris-Saclay

École doctorale n° 000, dénomination et sigle
Spécialité de doctorat: Physique
Unité de recherche: voir annexe
Référent: : voir annexe

Thèse présentée et soutenue à ....., le .... 2023, par

David SIMONNE

Composition du jury

Prénom Nom Titre, Affiliation	Président/e
Prénom Nom Titre, Affiliation	Rapportrice
Prénom Nom Titre, Affiliation	Rapporteur
Prénom Nom Titre, Affiliation	Examinatrice
Prénom Nom Titre, Affiliation	Examinateur
Prénom Nom Titre, Affiliationt	Examinateur

Direction de la thèse

Alessandro Coati Dr., Synchrotron SOLEIL	Directeur
Andrea Resta Dr., Synchrotron SOLEIL	Codirecteur
Marie-Ingrid Richard Dr., CEA Grenoble	Coencadrante

Contents

List of Figures

List of Tables

Chapter 1

Introduction

(The Introduction chapter should contain background information as appropriate, plus definitions of all special and general terms. Your topic should be: clearly stated and defined; have a clear overall purpose; and have clear, relevant and coherent aims and objectives. It is also informative to give a brief description of the contents of the remaining chapters of the thesis. This alerts the reader and prepares them for the rest of the thesis.)

1.1 The oxidation of Ammonia

Ammonia oxidation is an essential catalytic reaction used in the production of artificial fertilizers and in environmental applications. In both cases, particular focus is on two products of the reaction, namely, NO and N_2 . The selectivity toward either one is dictated by reaction parameters, that is, by temperature, NH_3 and O_2 partial pressures, and the type of catalyst.

Detail and literature about the oxidation of Ammonia on Platinum nano-catalyst can be found here (Resta et al. 2020).

1.1.1 From industry to model catalysis

"A long standing conundrum in the catalysis community emerged at the interface between surface science and heterogeneous catalysis, better known as the pressure and materials gap."

Nature Catalysis editorial, 2018.

	Pressure	Material	Temperature
Industry	1-12 bar	Wires ($\varnothing \approx 80\,\mu m$)	>1000 K
Literature	UHV, mbar	Single crystals	RT - 1000 K
This study	Near ambient pressure (0.5 bar)	Single crystals and nanoparticles	≈ 750 K

Table 1.1: Material and pressure gap in heterogenous catalysis.

1.1.2 Crystal structures

1.1.3 Pt 111

1.1.4 Pt 100

1.1.5 Nanoparticles

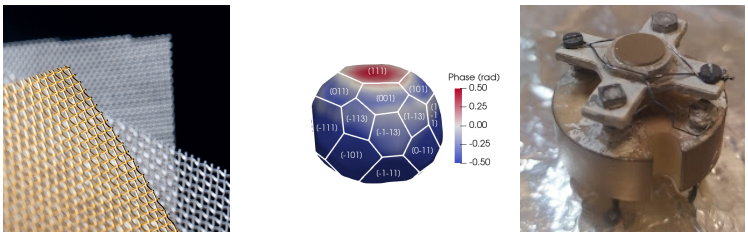

Figure 1.1: Platinum gazes used in industry (left), Pt particle measured at SixS, ⌀ is of about 300 nm (middle), Pt 111 single crystal used in SXRD and XPS experiments, ⌀ is of about 8 mm (right).

1.2 Aim and Scope

1.3 Outline of the Thesis

In the first chapter of this thesis we will come back to the basics behind each X-ray technique that was used to study the catalyst, as well as define the exact meaning of heterogeneous catalysis and how

In the second chapter we will present and discuss the results that we obtained with three different techniques

Chapter 2

Theory and methods

2.1 X-ray interaction with matter

Understanding the different mechanism at play when photons interact with matter is of crucial importance to be able to decide how to use X-rays as a probe in material science. Each phenomena is at the source of different techniques, diffraction brings surface X-ray diffraction (SXRD) and Bragg coherent diffraction imaging (BCDI), two techniques used in the frame of this thesis that give complementary information about the sample structure bulk and surface.

X-ray absorption together with the photoelectric effect explained by Einstein in 1905 are at the source of a third technique used, X-ray photoelectron spectroscopy, which yields information specific to the nature of the adsorbates on the sample's surface.

Technique	Sample	Sensitivity	Information
Bragg Coherent Diffraction Imaging (BCDI)	Pt nanoparticles (111), (110), (100), ...	Bragg electronic density	Shape, 3D strain and displacement arrays
Surface X-ray Diffraction (SXRD)	Pt single crystals (111), (100), (311)	Surface structure	Roughness, relaxation and crystallographic phases
X-ray Photoelectron Spectroscopy (XPS)	Pt single crystals (111), (100)	Surface species	Species presence, quantity, oxidation state

Table 2.1: Near-ambient pressure (NAP) X-ray techniques carried out at the SixS (SOLEIL) or B-07 (Diamond) beamlines

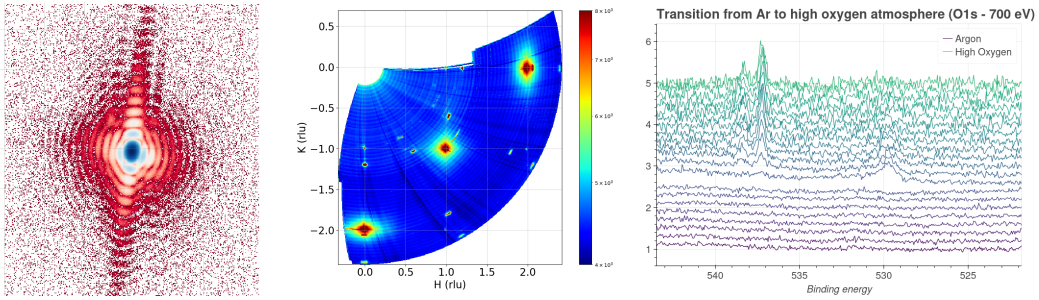

Figure 2.1: Slice of 3D diffraction pattern collected at the SixS beamline at the SOLEIL synchrotron (left). Reciprocal space map in HK plane collected at the SixS beamline at the SOLEIL synchrotron (middle). Ambient pressure XPS spectra collected during a transition between two atmospheres, collected at the B07 beamline at the Diamond synchrotron (right).

In this chapter we will discuss the origin of each technique from fundamentals that not only tailor their experimental design but also their operability and sensitivity.

2.1.1 Scattering from electrons and atoms

The duality between wave and particles was first mentionned by Max Planck and Albert Einstein in the early 20th century and generalized to all matter by Louis-Victor de Broglie in 1924 with the famous formula:

$$\lambda = \frac{h}{p} \tag{2.1}$$

Electromagnetic waves, i.e. light or photons can be characterized by their energy E in eV and wavelength λ in m. The conversion between is realized thanks to Planck's constant $h = 6.626 \times 10^{-34}$ J s and the speed of light in vacuum $c = 2.9979 \times 10^{8}$ m s^{-1} (eq. 2.2).

$$E = \frac{hc}{\lambda} \tag{2.2}$$

The properties of the photon and its use in our society depends on its energy and wavelength. If visible light is situated between 500eV and 900eV, micro-waves used in our everyday life are situated between 10^{-6}eV and 10^{-4}eV. On the other side of the electromagnetic spectrum, we have higher energy photons such as X-rays ($\in [10^2, 10^6]$eV) and γ-rays (above 10^{-6}eV).

X-rays have a wavelength of a few Å (10^{-10}m) making them the perfect probe to study the structures of materials at the atomic scale thanks to different interaction with matter.

Cross-sections

When an electromagnectic beam interacts with matter it will be attenuated by absorbtion, reflection or scattering. Each process can be quantified depending on the atoms (and thus on the electronic cloud) the beam interacts with and the energy on the incident photon, this is illustrated in figure 2.2. The cross-section for a particuliar process p is defined as follows (Willmott 2019):

$$\sigma_p = (\Lambda_p N_i)^{-1} \tag{2.3}$$

Λ_p is the attenuation length in m, i.e. the length after which the beam is reduced to $1/e$, N_i is the atomic number-density in atoms/unit volume.

Compton scattering, also named inelastic scattering, is a process during which some of the incident electromagnetic wave energy is transfered to the atoms' electrons. This results in a lower energy for the scattered photon (and therefore a higher wavelength) compared to the incident photon.

In the frame of this thesis, the (elastic) Thomson scattering cross-sections is the most important, at the origin of X-ray diffraction. This process is dominant for energies below 200keV, together with photoelectric absorption.

Scattering from an electron

We begin our discussion of X-ray scattering by considering scattering from a single free electron using classical electromagnetic theory. During elastic scattering, the oscillating electric field of the incident X-ray wave exerts an electromagnetic force on the electron, causing it to accelerate and oscillate in the same direction as the incident electronic field.

During an elastic scattering event, the oscillating electron emits a spherical electromagnetic wave with the same wavelength as the incident beam (Thomson scattering). The scattered field $\vec{E}_{scatt}$ is then proportional to the incident electromagnetic field $\vec{E}_{in}$ as follows (Jens Als-Nielsen 2011):

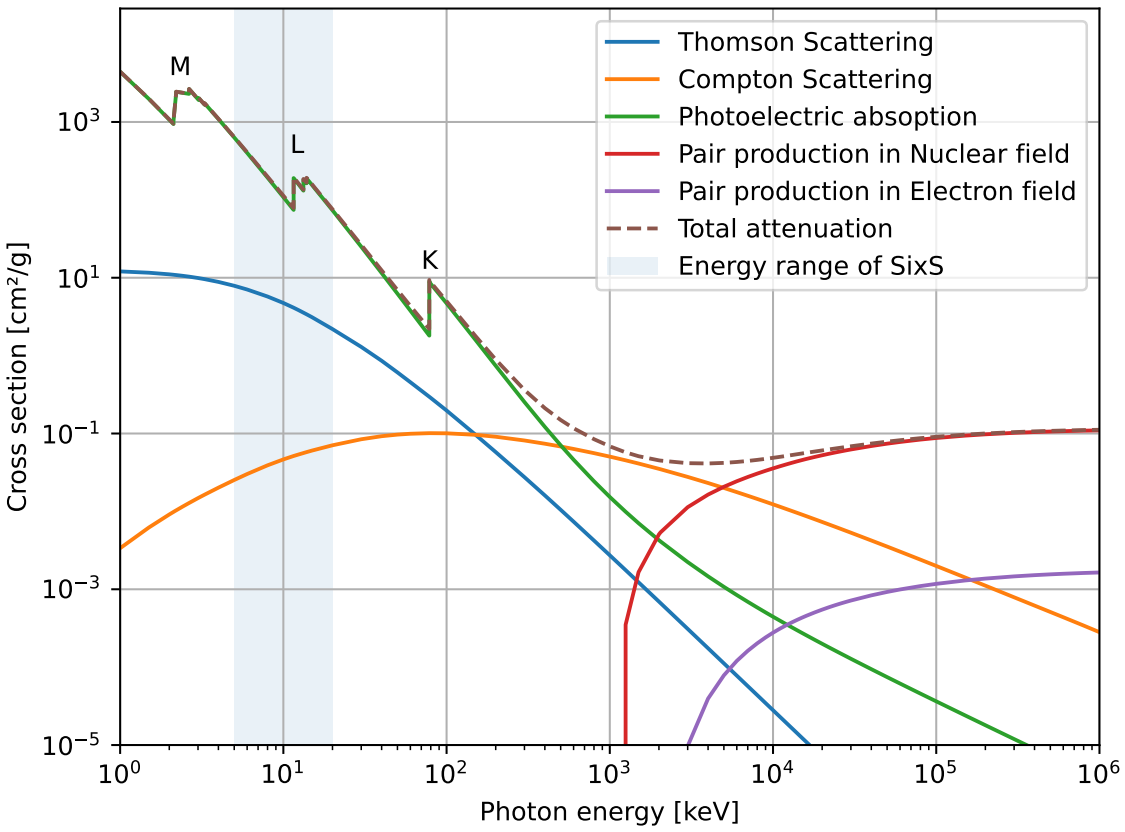

Figure 2.2: Cross-sections for Platinum (Z=78) for various processes that occur when photons interact with matter. The data was taken from the NIST (National Institute of Standards and Technology) (Berger et al. 2010) website. The energy range of the SixS beamline at SOLEIL is highlighted in blue.

$$\frac{\vec{E}_{scatt}(R,\,t)}{\vec{E}_{in}} = -r_0 \frac{e^{\vec{k}.\vec{R}}}{|\vec{R}|}|\hat{\epsilon}.\hat{\epsilon}'| \tag{2.4}$$

with $|\vec{R}|$ the distance at which the scattering is detected at the time t. r_0 is the Thomson scattering length defined as:

$$r_0 = \frac{e^2}{4\pi\epsilon_0 m_e c^2} \tag{2.5}$$

The minus sign illustrates a phase shift of π between the incident and scattered wave, $\hat{\epsilon}$ and $\hat{\epsilon}'$ are respectively the polarization vectors of the incident and scattered electromagnectic fields.

The differential cross-section for Thomson scattering measures the efficiency of the scattering in the volume occupied by a solid angle $d\Omega$ in the direction $\vec{R}$ (Jens Als-Nielsen 2011). It is defined as follows:

$$\frac{d\sigma_{ts}}{d\Omega} = \frac{|\vec{E}_{scatt}(R,t)|^2 R^2}{|\vec{E}_{in}|^2} \tag{2.6}$$

By substituting eq. 2.4 into eq. 2.6, it becomes clear that the scattering is proportional to the Thomson scattering length and that the intenisty is attenuated depending on the dot product between the two polarizations. The polarization factor P for scattered beams is defined as $P = |\hat{\epsilon}.\hat{\epsilon}'|^2$ and we can write the differential cross-section as:

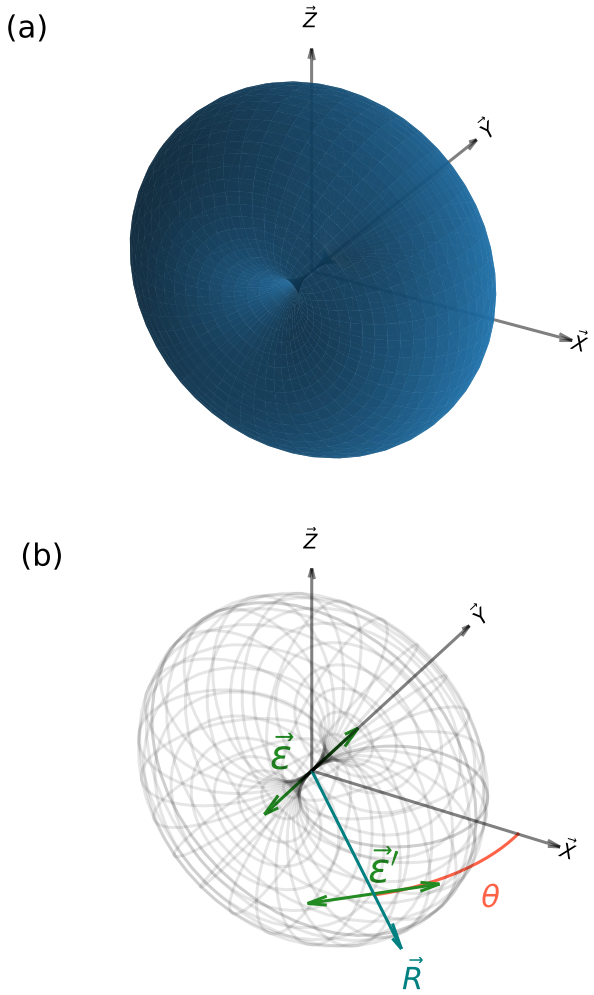

Figure 2.3: Effect of relation between synchrotron X-ray polarization $\hat{\epsilon}$ and scattered X-ray polarization $\hat{\epsilon}'$ on the scattered field. The scattered field intensity is attenuated by a $\cos\theta$ factor, where θ is the angle between the plane perpendicular to the electric field and the direction of observation $\vec{r}$. Working in the vertical plane is preferable to maximize the intensity of the scattered field, this has pratical repercussions in surface X-ray diffraction for which it is preferable to work in a vertical geometry to scan large 2D areas of the reciprocal space.

$$\frac{d\sigma_{ts}}{d\Omega} = r_0^2 |\hat{\epsilon}.\hat{\epsilon}'|^2 = r_0^2 P \tag{2.7}$$

The effect of the polarization of the incident beam is illustrated in figure 2.3. At synchrotron sources where the incident beam is horizontally polarized, working in the vertical plane becomes more effective since the polarization factor is always equal to one.

The total cross-section for the scattering event by a single free electron can be computed by integrating the differential cross-section over all the possible scattering angles, ie. by averaging all possible polarization directions (Willmott 2019). This yields $\sigma_{ts} = 8\pi r_0^2/3 = 0.665$b, the total Thomson scattering cross-section is constant, independant of the incoming photon energy. This results holds for X-rays for which the scatterer i.e. the electron can be considered as free (Willmott 2019).

Scattering from a single atom

As we have seen the main scatterer for Thomson scattering is the electron. The scattering of the incident beam from an atom is therfore proportional to the electronic density $\rho_{atom}(\vec{r})$. For a single atom of atomic number Z we have :

$$\int \rho_{atom}(\vec{r})d\vec{r} = Z \tag{2.8}$$

The scattering amplitude shows a dependance depending on the wavelength of the incident beam λ, and on the direction of detection defined by the scattering angle 2θ between the wavevector of the incident photon $\vec{k_i}$ and the wavevector of the scattered photon $\vec{k_s}$ (fig. 2.4).

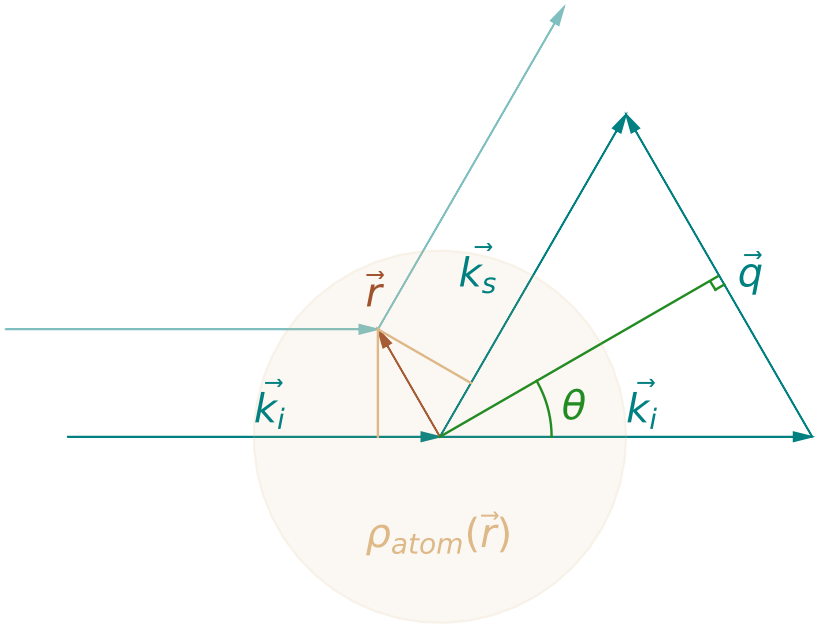

Figure 2.4: Geometry of the momentum transfer $\vec{q}$ in reciprocal space, 2θ is the scattering angle.

This leads to the definition of the momentum transfer, $\vec{q}$, to describe the amplitude of a scattering event (eq. 2.9, fig. 2.4).

$$\vec{q} = \vec{k_i} - \vec{k_s} = 2|\vec{k}|\sin\theta = \frac{4\pi}{\lambda}\sin\theta \tag{2.9}$$

The phase difference between a wave scattered at a position $\vec{O}$ and a wave scattered at a position $\vec{O} + \vec{r}$ is equal to $(\vec{k_i} - \vec{k_s}).\vec{r} = \vec{q}.\vec{r}$ (fig. 2.4). We assume here that the scattering event is elastic ($|\vec{k_i}| = |\vec{k_s}|$) and that the waves are plane waves parallel to each other when in the small scattering volume dr.

A small volume dr will have a contribution equal to $-r_0\rho(\vec{r})dr$ to the scattered field with a phase $e^{i\vec{q}.\vec{r}}$.

By integrating over the volume occupied by the atom we obtain the total contribution of an atom to the scattered field in the direction 2θ:

$$-r_0 \int \rho(\vec{r}) e^{i\vec{q}.\vec{r}} d\vec{r} = -r_0 f(\vec{q}) = -r_0 FT[\rho(\vec{r})] \tag{2.10}$$

The scattering amplitude as a function of $\vec{q}$ is described by the atomic scattering factor $f(\vec{q})$, which is defined as the fourier transform of the electronic density $\rho(\vec{r})$. This hypothesis is at the basis of several techniques such as Bragg coherent diffraction imaging for which the use this hypothesis to compute the scattered amplitude from the fourier transform of the electronic density (sec. X).

The values for the atomic scattering factor can be calculated using tabulated coefficients (eq. 2.11) available online (Brown et al. 2006). The intensity decreases with $\vec{q}$ as illustrated in figure 2.5.

$$f(\vec{q}) = \sum_{i=1}^{4} a_i \exp(-b_i(\frac{q}{4\pi})^2) + c \tag{2.11}$$

The scattering intensity is equal to the square of the scattering amplitude. For example, the scattering intensity of palladium atoms at $|\vec{q}| \approx 2.75$Å is only $\approx 31\%$ of that of platinum atoms. In the case of oxygen, the intensity falls down to $\approx 6.7\%$. This difference in scattering intensity between elements becomes crucial when working with small objects that have a small scattering volume such as nanoparticles, as in Bragg Coherent Diffraction Imaging.

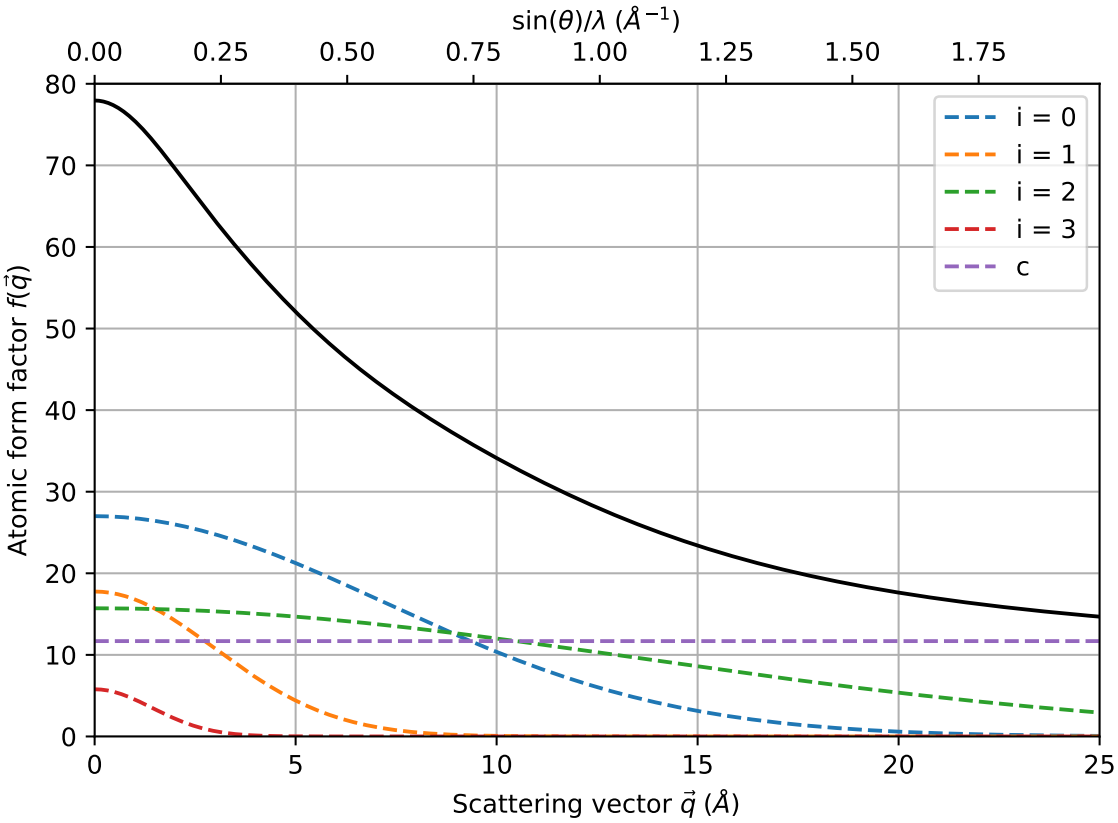

Figure 2.5: Atomic form factor calculated for Pt (Z=78) using tabulated values from Brown et al. 2006 for equation 2.10. The scattering intensity decreases with the scattering angle θ but increases with the incident wavelength λ. i and c respectively designate the Gaussian contribution and constant in eq. 2.11.

2.1.2 Scattering from atoms and molecules

In the case of multiple atoms, each atom can be described as a small volume dr in the electronic density, and the scattered field by the superposition of the contribution from the electronic cloud surrounding the atoms.

Furthermore, we assume that the source and detector are sufficiently far from the charge distribution so that the incident and scattered X-rays may be represented as plane waves, parallel to each other and perpendicular to the direction of propagation. This is the so-called far-field limit or the fraunhofer region.

In the scattering direction defined by the angle 2θ between k_f and k_i

Finally, we assume that the charge distribution is small and that the scattering is weak so that the sample can be treated as a simple "perturbation" to the incident beam resulting in a linear problem (Jens Als-Nielsen 2011) and that the Born approximation is valid.

Working under these assumption is known as kinematic diffraction for which we can easily derive the intensity of the scattered photons. We therefore ignore multiple-scattering of photons inside the sample and xxx. This is correct when working with low incident angles and penetration depths as for example in surface X-ray diffraction (see Section x).

2.1.3 Coherence

2.1.4 Bragg's Law

The lattice of our crystal is defined by three vectors $\vec{a}$, $\vec{b}$, $\vec{c}$. Any vector $\vec{v}$ of the unit cell can then be created by a linear combination of these three vectors:

$$\vec{v} = n_1\vec{a} + n_2\vec{b} + n_3\vec{c}, \quad with\ (n_1, n_2, n_3) \in \mathbb{Z}^3 \tag{2.12}$$

the volume of the unit cell is:

$$V = \vec{a}.(\vec{b} \times \vec{c}) \tag{2.13}$$

An important tool of crystallography is the *reciprocal space* of dimension m^{-1}, defined by the three vectors $\vec{a*}$, $\vec{b*}$, $\vec{c*}$:

$$\vec{a^*} = \frac{2\pi}{V}(\vec{b} \times \vec{c}), \qquad \vec{b^*} = \frac{2\pi}{V}(\vec{c} \times \vec{a}), \qquad \vec{c^*} = \frac{2\pi}{V}(\vec{a} \times \vec{b}) \tag{2.14}$$

$\vec{q}$ can be written as a linear combination of the reciprocal length between planes.

$$\vec{Q} = n\frac{2\pi}{d_{hkl}}, \qquad with\ n \in \mathbb{Z} \tag{2.15}$$

Combining (**??**) and (2.15), we fall back on the most famous equation of crystallography, Bragg law:

$$n\lambda = 2d_{hkl}\sin\theta \tag{2.16}$$

To summarize, a Bragg peak result from the constructive interference between coherently scattered waves at discrete values of the incident angle 2θ or of the momentum transfer $\vec{q}$ on a specific set of crystalline planes. $\vec{q}$ and 2θ are linked through (**??**). The condition to have constructive interference is known as Bragg law and is given by (2.16).

From (2.15), one can define the general reciprocal-space metric tensor for any crystalline system:

$$\frac{(2\pi)^2}{d_{hkl}^2} = h^2\,(\vec{a^*}.\vec{a^*}) + k^2\,(\vec{b^*}.\vec{b^*}) + l^2\,(\vec{c^*}.\vec{c^*}) + 2hk\,(\vec{a^*}.\vec{b^*}) + 2hl\,(\vec{a^*}.\vec{c^*}) + 2kl\,(\vec{b^*}.\vec{c^*}) \quad (2.17)$$

$$\frac{(2\pi)^2}{d_{hkl}^2} = h^2\,a^{*2} + k^2\,b^{*2} + l^2\,c^{*2} + 2hk\,a^*.b^*\cos\gamma^* + 2hl\,a^*.c^*\cos\beta^* + 2kl\,b^*.c^*\cos\alpha^* \quad (2.18)$$

$$\frac{(2\pi)^2}{d_{hkl}^2} = Ah^2 + Bk^2 + Cl^2 + Dhk + Ehl + Fkl \quad (2.19)$$

Equation (2.17) can be simplified as (2.20) for a simple cubic system, defining the interplanar spacing between the crystalline planes:

$$d_{hkl} = \frac{2\pi}{|\vec{a^*}|\sqrt{h^2+k^2+l^2}} = \frac{|\vec{a}|}{\sqrt{h^2+k^2+l^2}} \quad (2.20)$$

Moreover, for each peak, indexed by its *hkl* miller indices that specify the orientation of the crystalline planes, the momentum transfer can be written as a linear combination of reciprocal space vectors, for a cubic lattice:

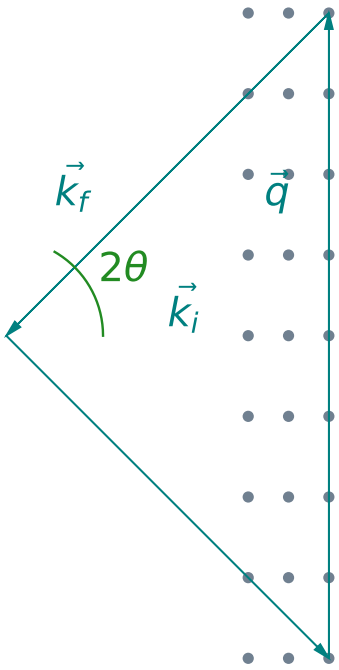

Figure 2.6: Geometry of the momentum transfer $\vec{q}$ in reciprocal space, 2θ is the scattering angle.

The figure **??** leads to (**??**) and illustrates the particular case of a Bragg peak. If the momentum transfer $\vec{q}$ can be expressed as a linear combination of reciprocal vectors, here graphically verified, a Bragg peak occurs for this value of Q.

$$\vec{Q_{hkl}} = h\vec{a*} + l\vec{b*} + k\vec{c*} \quad (2.21)$$

2.1.5 Intensity of a Bragg peak

Neglecting absorption, the intensity of a Bragg peak I_{nuc} as a function of its miller indices hkl and of 2θ can be written as:

$$I_{nuc} = A \times |F_{hkl}|^2 \times j_{hkl} \times L(2\theta) \times \exp(-2W) \tag{2.22}$$

where A is an instrument constant.

Structure factor

F_{hkl} is known as the structure factor, it is given by:

$$F_{hkl} = \sum_{j=0}^{n} b_j \exp(-2\pi i \vec{Q}.\vec{r_{j0}}) \tag{2.23}$$

The structure factor is the summation of the contribution to the scattering energy of each atoms at the position $\vec{r_{j0}}$ of scattering length b_j in our unit cell for a given $\vec{Q}$. The position of the atom $\vec{r_{j0}}$ is given by:

$$\vec{r_{j0}} = x_j\vec{a} + y_j\vec{b} + z_j\vec{c} \tag{2.24}$$

Debye-Waller factor

The position $\vec{r_j}$ of the atom j is not static but should be rather understood as the instantaneous position of the atom. In a crystal, atoms vibrate around their equilibrium position $\vec{r_{j0}}$, we have:

$$\vec{r_j}(t) = \vec{r_{j0}} + \vec{u}(t) \tag{2.25}$$

$\vec{u} = \vec{u}(t)$ is the thermal displacement, accounting for thermal vibrations in the crystal. These oscillations around the equilibrium position can be understood following the model of a harmonic oscillator at low temperature, with discrete frequencies of vibrations. The frequency of the vibrations, that increase with temperature, are linked to quasi-particles named *phonons*. Another contribution to the thermal displacement is the zero-point displacement, if one could lower the temperature of the crystal in a perfect vacuum down to absolute zero, one would have expected the system to not show any motion. However, quantum physics tells us that even at absolute zero there is a probability for the atom to not be in at its equilibrium position, called zero-point displacement. Moreover, the Debye-Waller factor also takes into account the static displacement in the lattice that is linked to disorder. This will be discusses further in chapter 2.

The exponential in (2.23) can be rewritten as:

$$\exp(-2\pi i\vec{Q}.\vec{r_j}) = \exp(\ -2\pi i\vec{Q}.(\vec{r_{j0}} + \vec{u})\ ) \tag{2.26}$$

The average of this equation is given by:

$$\langle \exp(-2\pi i\vec{Q}.\vec{r_j}) \rangle = \exp(-2\pi i\vec{Q}.\vec{r_{j0}}) \times \langle \exp(\ -2\pi i\vec{Q}.\vec{u})\ \rangle \tag{2.27}$$

The second term of this expression can be expanded as the second order Taylor series for $\exp x_0$ with $x_0 = -2\pi i\vec{Q}.\vec{u}$ at zero, we loose the (2π) for clarity:

$$\langle \exp(-i\vec{Q}.\vec{u}) \rangle = 1 - \langle\ i\vec{Q}.\vec{u}\ \rangle - \frac{1}{2}\langle\ (\vec{Q}.\vec{u})^2\ \rangle + o\ (\ \langle\ (\vec{Q}.\vec{u})^2\ \rangle\ ) \tag{2.28}$$

Since the displacement are random, the average of $i\vec{Q}.\vec{u}$ is equal to zero. However the average of the square of $\vec{Q}.\vec{u}$ is non zero and can be further developed as:

$$\langle\ (\vec{Q}.\vec{u})^2\ \rangle = Q^2\ \langle\ u^2\ \rangle\ \langle\ \cos\theta^2\ \rangle = \frac{1}{3}\ Q^2\ \langle\ u^2\ \rangle \tag{2.29}$$

which leads to:

$$\langle \exp\left(-i\vec{Q}.\vec{u}\right)\rangle = 1 - \frac{1}{6}\ Q^2\ \langle\ u^2\ \rangle \tag{2.30}$$

that corresponds to the first order Taylor series for $\exp x_0$ with $x_0 = \frac{1}{6}\ q^2\ \langle\ u^2\ \rangle$ at zero, we can write:

$$1 - \frac{1}{6}\ Q^2\ \langle\ u^2\ \rangle = \exp\left(\frac{1}{6}\ Q^2\ \langle\ u^2\ \rangle\ \right) \tag{2.31}$$

The final intensity contribution of the Debye Waller factor is the square of (2.31) given by:

$$\exp\left(\frac{1}{3}\ Q^2\ \langle\ u^2\ \rangle\ \right) \tag{2.32}$$

The last two terms of (2.22), respectively j_{hkl} and $L(2\theta)$ are the multiplicity of a Bragg peak and the Lorentz factor. They will be studied in a section covering the instrument used for powder diffraction for they both relate more to the collection of the data than to the theoretical intensity of a Bragg peak.

Lorentz factor

Explain here how we actually collect the data

Ewald sphere is quite important here.

Multiplicity

Small introduction to space groups ?

Bibliography

Resta, Andrea et al. (2020). 'Ammonia Oxidation over a Pt25Rh75(001) Model Catalyst Surface: An Operando Study'. In: *Journal of Physical Chemistry C* 124.40, pp. 22192–22199. ISSN: 19327455. DOI: 10.1021/acs.jpcc.0c07128.

Willmott, Philip (2019). *An Introduction to Synchrotron Radiation: Techniques and Applications*. John Wiley and Sons, Ltd. DOI: 10.1002/9781119280453.

Berger, M.J. et al. (2010). *NIST Standard Reference Database 8 (XGAM)*. DOI: https://dx.doi.org/10.18434/T48G6X. URL: https://www.nist.gov/pml/xcom-photon-cross-sections-database (visited on 15/06/2023).

Jens Als-Nielsen, Des McMorrow (2011). *Elements of Modern X-ray Physics*. John Wiley and Sons, Ltd. DOI: 10.1002/9781119998365.

Brown, P. J. et al. (2006). *International Tables for Crystallography*. Vol. C. Chap. 6.1, pp. 554–595. DOI: 10.1107/97809553602060000600.

université PARIS-SACLAY

ÉCOLE DOCTORALE
Physique en île de France
(PIF)

Titre: Propriétés catalytiques à l'échelle nanométrique sondées par diffraction des rayons X de surface et imagerie de diffraction cohérente
Mots clés: Diffraction, Catalyse, Surface, Structure, Déformation

Résumé: Le principal objectif est d'imager des nanostructures pour sonder les conditions in situ et operando ; mesurer la structure à l'échelle nanométrique et révéler également les effets de masse, de surface et d'interface ainsi que les défauts. Viser à terme à comprendre les phénomènes structurels importants pour les nanocatalyseurs et les relier à leur activité, sélectivité, réutilisabilité et durabilité. En complément des études cohérentes aux rayons X sur des particules individuelles, des techniques étudiants la moyenne des ensembles comme la diffraction des rayons X à incidence rasante seront employées pour voir si l'évolution des formes d'ensemble sont similaires à celles des nanoparticules uniques et sondent s'il y a une déconnexion entre les particules uniques et l'activité catalytique sur des billions de particules. La catalyse des nanomatériaux est apparue comme un moyen efficace d'exposer une surface plus élevée et d'accélérer les processus catalytiques en maximisant le rapport surface-volume. Le développement d'une catalyse hétérogène avec une sélectivité ciblant les 100% est un défi constant ainsi que la compréhension de la durabilité et du vieillissement du catalyseur lui-même. Dans un procédé réel (réacteur d'usine de catalyseur, échappement de voiture, pile à combustible), l'évolution de la forme et de la déformation des nanoparticules catalytiques dans des conditions de réaction contribue au vieillissement du catalyseur et a un impact sur la durée de vie du dispositif. Cependant, le processus catalytique et les changements structurels associés restent encore mal compris. Comprendre comment la structure du catalyseur est affectée par la couche adsorbée dans des conditions de réaction est donc de la plus haute importance pour formuler des relations de performance de structure de catalyseur qui guident la conception de meilleurs catalyseurs.

Title: Catalytic properties at the nanoscale probed by surface X-ray diffraction and coherent diffraction imaging
Keywords: Diffraction, Catalysis, Surface, Structure, Strain

Abstract: The main objective is to image nanostructures to probe in situ and operando conditions; measure the structure at nanoscale and to reveal bulk, surface and interface effects, as well as defects. Ultimately aiming to understand the structural phenomena important for the working nanocatalysts and link them to their activity, selectivity, reusability and sustainability. In complement to coherent x-ray studies on individual particles, ensemble-averaging techniques like grazing incidence x-ray diffraction will be employed to see if the evolution of ensemble shapes is similar to the one of single nanoparticles and probe if there is a disconnect between single particles and the catalytic activity over trillions of particles. Catalysis of nanomaterials has emerged as an efficient way to expose higher surface area and accelerate catalytic processes by maximizing the surface-volume ratio. The development of heterogeneous catalysis with selectivity targeting the 100% is a constant challenge as well as understanding the durability and ageing of the catalyst itself. In a real process (catalyst plant reactor, car exhaust, fuel cell) the shape and strain evolution of catalytic nanoparticles under reaction conditions contributes to the ageing of the catalyst and impact the lifetime of the device. However, the catalytic process and the associated structural changes remain poorly understood. Understanding how catalyst structure is affected by the adsorbed layer under reaction conditions is therefore of utmost importance to formulate catalyst structure performance relations that guide the design of better catalysts.

Maison du doctorat, Université Paris-Saclay
2e étage, aile ouest, École normale supérieure Paris-Saclay
4 avenue des Sciencs
91190 Gif-sur-Yvette, France